Disentangling the biotic and abiotic drivers of evapotranspiration in a degraded raised bog

Vincent E. Flemming[1], Nicolas Behrens[1], Mana Gharun[1]

[1]Institute of Landscape Ecology, University of Münster, Münster, D-48149, Germany

Correspondence to: Vincent E. Flemming (vincent.flemming@uni-muenster.de)

Abstract. Latent heat flux (LE) – the energy required for evapotranspiration – plays a major role in determining the capacity of ecosystems for cooling the climate. Given the major role that LE plays in linking water, energy, and carbon cycles, it is important to understand the drivers of LE and how they interact with one another across different time scales. However, the interaction between abiotic (e.g., atmospheric and soil meteorological conditions) and biotic (e.g., canopy conductance (g_c), gross primary productivity (GPP)) drivers on LE remains insufficiently understood, particularly in the context of drained peatlands dominated by heath and dwarf-shrub vegetation. Here, we analysed eddy covariance measurements collected over three years between 2023 and 2025 at a drained raised bog in northwest Germany. Using high frequency CO_2, H_2O, energy flux, and meteorological measurements we 1) explored the daily and seasonal dynamics of LE, 2) quantified the influence of biotic and abiotic drivers on LE, and 3) determined the vegetation physiological thresholds at which g_c limits LE due to an increase in atmospheric and soil dryness. To disentangle the biotic and abiotic controls of LE, we derived a continuous time series of g_c by inverting the Penman-Monteith equation using 30-minute LE fluxes measured with the eddy covariance method, which were also aggregated to daily values. This approach enabled us to estimate daily and subdaily g_c alongside GPP and continuous daily meteorological variables, including net radiation (R_n), air temperature (T_a), vapor pressure deficit (VPD, i.e., atmospheric dryness), groundwater table depth (WTD), and soil water content (SWC, i.e., soil dryness). Using daily mean data, detrending of mean seasonality, and removal of time lag, the variable component of the drivers was extracted and the effect size on LE was determined. R_n and GPP showed the largest effect on LE, with marked differences in their effect during the growing season versus the non-growing season. During the growing season R_n and GPP have the largest effect on LE, while outside the growing season, WTD and VPD have the greatest impact. g_c which was estimated from the inverted Penman-Monteith model at the daily and sub-daily (30-min) scale, responded strongly to VPD but not to SWC. The peak of a local polynomial regression indicated the thresholds for VPD and SWC at which LE was limited by vegetation physiological responses (g_c). With increase in atmospheric dryness, g_c significantly limited LE above a VPD threshold of 7.6 hPa at the subdaily scale, and at a threshold of 4.6 hPa at the mean daily scale. These results help us better understand the potential impacts of environmental conditions on the evaporative cooling capacity of drained peatlands. Further research is needed to understand how occurrence of extreme climatic conditions will affect the relationships identified in this study.

1 Introduction

Evapotranspiration (ET) is a key component of the land water cycle as a large portion of water reaching land via precipitation (P) is removed through ET (Türk et al., 2026; Wilusz et al., 2017). ET is the transfer of water from surface (evaporation) and vegetation (transpiration) into the atmosphere, whereby liquid or solid water transforms into water vapor. The phase change of water requires energy, which is transported away as latent heat flux (LE), thereby cooling the land surface. ET and LE are thus directly related, with LE representing the energy equivalent of ET. Vegetation transpiration exchanges water vapor for CO_2, making ET a key link between water cycle, energy cycle, and carbon cycle. Beyond their role in greenhouse gas uptake and carbon sequestration, the climate mitigation potential of natural ecosystems is therefore also strongly determined by their evaporative cooling capacity. Through ET-driven LE exchange, ecosystems can moderate surface temperatures, reduce heat extremes, and influence regional climate conditions, highlighting that the climate benefits of ecosystem restoration and conservation extend beyond carbon storage alone (Miralles et al., 2025).

Although peatlands cover only 3% of global land area, they have a significant climate potential as they store around 30% of global terrestrial soil organic carbon (Yu, 2012). In their natural state peatlands are (nearly) waterlogged ecosystems that naturally sequester and store carbon for centuries. Anthropogenic drainage for agriculture, peat cutting and forestry as well as climate change effects lead to lowered water tables, degradation of the peat and emission of the carbon as CO_2. Lowered water tables reduce the water-holding capacity of the porous peat matrix, enhancing lateral water loss and altering vertical water vapor fluxes from ET (Liu et al., 2022). Vegetation change further amplifies these dynamics. In degraded peatlands, increased shrubification and dominance of woody vegetation can change transpiration rates, intensifying or lowering vertical water losses (Limpens et al., 2014). Intact peatlands possess hydrological self-regulation mechanisms that mitigate drought effects (Nijp et al., 2017). Their high water-holding capacity also makes them key regulators of hydrology, buffering both water availability (Karimi et al., 2024) and the impact of droughts (Kettridge and Waddington, 2014). However, these capacities are impaired when water levels decline.

In drained peatlands vegetation cover often shifts from mosses to heath dwarf-shrub vegetation. Vascular plants can actively regulate transpiration by opening and closing their stomata. The strategies plants have for responding to soil and air dryness vary among species (Morgan et al., 2025; Fu et al., 2022). Previous experiments in controlled environments show that transpiration in *Calluna vulgaris* and *Molinia caerulea* (vegetation that dominate our peatland of study) increases with rising vapor pressure deficit (VPD) under moist soil conditions (Gobin et al., 2015). These experiments also show that when soil is dry, transpiration of *C. vulgaris* initially increases with rising VPD, but decreases after a certain dryness point. Meanwhile *M. caerulea* shows no change in transpiration with increasing VPD under dry soil conditions (Gobin et al., 2015). These observations indicate variation in the strength of stomatal regulation among vegetation types, highlighting the complex role of vegetation in controlling transpiration. This variability can lead to contrasting effects on LE under conditions of increased warming and drying (Massmann et al., 2019).

Net radiation (R_n), VPD, air temperature (T_a), groundwater table depth (WTD), and soil water content (SWC) are known to be the key abiotic drivers of LE, with R_n consistently identified as the dominant driver of LE (e.g., Alekseychik et al., 2017 (raised bog, boreal); Gunawardhana et al., 2021 (alpine sphag. valley bog); Sonnentag et al., 2010 (minerotrophic fen, boreal)). In contrast, the influence of WTD is more complex: some studies report that WTD is only significantly correlated with LE under specific hydrological conditions, such as when WTD is very close to or above the soil surface (Humphreys et al., 2006; Gunawardhana et al., 2021; Lafleur et al., 2005). Biotic drivers include photosynthesis at the canopy scale expressed as gross primary productivity (GPP), as well as the degree to which vascular plants regulate transpiration through stomatal opening and closure, represented by canopy conductance (g_c). Through these processes, vegetation can exert a stronger control on LE than the peatland type itself (Humphreys et al., 2006).

Despite the overarching energy limitation imposed by R_n, the roles of other drivers, such as WTD and vegetation composition, remain variable and insufficiently resolved, particularly in Central European peatlands where direct energy flux measurements are still limited. While the effects of abiotic controls (e.g., VPD) on LE are well established from a physical perspective, their interactions with biotic factors mean that the magnitude and direction of their influence on LE can vary depending on both their intensity and the prevailing vegetation composition.

Peatland conservation measures, including rewetting and vegetation management practices such as tree removal, are widely implemented across Central Europe and can directly influence LE. To identify effective conservation and restoration strategies, it is therefore essential to improve our understanding of the magnitude of these effects and the interactions among the factors controlling LE. In addition to active management, anthropogenic climate change is expected to alter peatland vegetation composition, potentially promoting shifts toward more shrubby vegetation even in the absence of direct human intervention (Heijmans et al., 2013). Such vegetation shifts are facilitated by lowered water levels and increasing temperatures (Heijmans et al., 2013) both of which are expected to intensify under future climate conditions (Shekhar et al., 2024). Understanding the interactions between biotic and abiotic controls on LE is thus critical for predicting how peatland carbon and water cycling will respond to climate change and associated shifts in environmental drivers.

In this study, we aimed to 1) investigate the diurnal and seasonal dynamics of LE measured directly using the eddy covariance (EC) method, 2) quantify the relative influence of biotic (GPP, g_c) and abiotic drivers (R_n, VPD, T_a, WTD, SWC) on LE, and 3) identify physiological thresholds at which canopy response to environmental conditions constrains LE.

Ecosystem-scale water vapor fluxes at high temporal resolution are most accurately captured using the EC technique, which directly measures gas exchange between the land surface and the atmosphere. Accordingly, we analyzed three full years of EC and micrometeorological observations from a drained bog ecosystem in northwestern Germany.

2 Methods

2.1 Study site

The study area is located in Amtsvenn-Hündfelder Moor (DE-Amv), North Rhine-Westphalia – Germany (52.17 °N, 6.95 °E, 38 m a.s.l.). This peatland covers an area of 894 ha (Europäische Union, 2021) and has been part of the Natura 2000 network since 2004, which is the world's largest contiguous network of protected areas (Directorate-General for Environment, 2024). The peatland is characterized as degraded raised bog dominated by *Calluna vulgaris* (L.) Hull, *Erica tetralix* L. and *Molinia caerulea* (L.) Moench. Species such as *Somatochlora arctica* Zetterstedt or *Drosera intermedia* Hayne occur here, making the ecosystem a valuable habitat (Utikal and Rückriem, 2019). According to the Köppen-Geiger climate classification, DE-Amv belongs to type Cfb (warm temperate, fully humid zone with warm summers) (Kottek et al., 2006). The average annual temperature (2007–2024, DWD, 2022) is 10.6 °C, with the coldest month being January with an average temperature of 1.1 °C and the warmest month being July with 18.3 °C. Mean annual P is 794 mm (2007 – 2024). The EC setup was installed in October 2022 at a height 2.8 m above the surface. DE-Amv is an official ICOS associate station.

2.2 Data

Data used in this study spans the period between 1 January 2023 and 31 December 2025. EC data was processed according to standard procedures, including filtering for low u^* conditions and spike removal (Pastorello et al., 2020). A detailed list of all available variables and measuring devices used can be found in Table 1. Missing data in meteorological variables was filled from a small meteorological ancillary tower, located 20 m from the EC tower. Additional remaining gaps were filled with XGBoost (Chen and Guestrin, 2016). Results of the gap-filling were verified on test datasets left out during model training and R^2 scores exceeded 0.85 for all gaps, except for incoming longwave radiation and SWC, where R^2 exceeded 0.7 for gap lengths of 40 days. Nighttime partitioning of CO_2 fluxes into GPP and ecosystem respiration (Reco) was done using the REddyProc package in R (Wutzler et al., 2018). The complete list of variables measured at the site is proved in Table 1.

Table 1: Included variables, measuring devices used and unit of the variables.

Variable	Device	Unit
H_2O	LI7200RS gas analyzer	µmol s^{-1} m^{-2}
wind speed, wind direction	Gill HS50 sonic anemometer	m s^{-1}, °
T_a	Vaisala HMP155	°C
relative humidity (rH)	Vaisala HMP155	%
radiation (R)	Kipp&Zonen CNR4	W m^{-2}
(–5 cm) soil temperature (T_s)	Soil T. Thermistor 7900-180	°C

(–5 cm) soil heat flux (SHF)	Hukseflux HFP10SC	W m^{-2}
(–5 cm) SWC	Stevens Hydraprobe	m^3 m^{-3}
P	TR-525M	mm
WTD	RXMOD-W1	cm

115

2.3 Energy balance

To evaluate the quality of the eddy covariance measurements, we evaluated the surface energy balance for the study site. Energy balance closure was calculated using the following equation, excluding the effects of snow:

$$E = R_n - SHF - LE - H \ . \quad (1)$$

120 E represents the error that consists of missing parameters and measurement errors. The sign convention here is that SHF, LE and H are positive upwards, and R_n is positive downwards. The energy balance was calculated using 30-minute measured data without gap filling.

2.4 Growing seasons identification

The growing season was identified on an annual basis using GPP. Start and end of the growing season were determined by 125 fitting a double sigmoid function to the partitioned GPP. Start and end of the growing season were determined as the first maximum and last minimum of the third derivative of a double sigmoid function (Beck et al., 2006).

2.5 Sub-daily and daily time series of canopy conductance

g_c was modeled in a modified way according to Runkle et al. (2014), which used the inversed Penman-Monteith equation. The Penman-Monteith equation includes surface conductance as a variable instead of g_c. Surface conductance is the sum of g_c, 130 soil evaporation and canopy interception evaporation. During the growing season, soil evaporation can be neglected; furthermore, data was filtered by P, to exclude interception evaporation, such that surface resistance ≈ g_c can be assumed (Matos et al., 2025; Gharun et al., 2020). g_c was first calculated by inverting the Penman-Monteith equation ($g_{c,PM}$), for days where no P on this day and less than 2 mm P the day before occurred (D = {I | P(i)=0 mm P(i-1) < 2 mm}, where D is the set of days used and i is the index of the days) (Dingman, 2015):

135 $$g_{c,PM} = \frac{g_{at}}{\left(\frac{\Delta(R_n - SHF) + \rho_a c_a g_{at} e_a^*(1-rH)}{ET \rho_w \lambda_v}\right)/\gamma - 1}, \quad (2)$$

with g_{at} [m s-1] as atmospheric conductance, λ_v [MJ kg^{-1}] is the latent heat of vaporization, γ [kPa K^{-1}] is called the psychrometric constant, although it is not a constant (Loescher et al., 2009), c_a [MJ kg^{-1} K^{-1}] is the heat capacity for air, Δ [kPa K^{-1}] is the slope of relation between saturation vapor pressure (VP) and T_a, e_a^* [kPa] is the saturation VP, ρ_a [kg m^{-3}] is

air density and ρ_w [kg m^{-3}] is water density, and c_a [MJ kg^{-1}] is the heat capacity of air. These values were calculated using the following equations (Dingman, 2015):

$$g_{at} \equiv \frac{v_a}{6.25\left(\ln\left(\frac{z_{veg}+2-0.7z_{veg}}{0.1z_{veg}}\right)\right)^2}, \quad (2a)$$

$$\lambda_v = 2.5 - 2.36 \cdot 10^{-3} T_a, \quad (2b)$$

$$\gamma \equiv \frac{c_a p_a}{\lambda_v \cdot 0.622}, \quad (2c)$$

$$c_a = 1.005 \cdot 10^{-3} + 1.82 \cdot 10^{-3} \cdot \frac{1801.6}{8314.3} \cdot \frac{rH6.1078 \cdot 10^{mT_a/m+T_a}}{T_a+273.15}$$

$$\begin{cases} \forall T_a \geq 0,\ m = 7.5,\ n = 237.4 \\ \forall T_a < 0,\ m = 7.6,\ n = 240.7 \end{cases}, \quad (2d)$$

$$\Delta \equiv \frac{2508.3}{(T_a+237.3)^2} \exp\left(\frac{17.3T_a}{T_a+237.3}\right), \quad (2e)$$

$$e_a^* = 0.611 \exp\left(\frac{xT_a}{T_a+y}\right)$$

$$\begin{cases} \forall T_a \geq 0,\ x = 17.27,\ y = 237.3 \\ \forall T_a < 0,\ x = 21.87,\ y = 265.5 \end{cases}, \quad (2f)$$

$$\rho_a = \frac{10^3(p_a - e_a^* rH)}{287.058(T_a+273.15)} + \frac{10^3 e_a^* rH}{461.495(T_a+273.15)}, \quad (2g)$$

$$\rho_w = 1000. \quad (2h)$$

z_{veg} [m] stands for the vegetation height while m and n are constants, and exp refers to Euler's number. The inverted Penman-Monteith equation assumes that no energy is stored temporarily (for example, by heating the soil above the SHF sensors). The problem described can be minimized by averaging EC data to daily values. Averaging data to daily values causes the diurnal information to be lost. Here, $g_{c,PM}$ was calculated with daily mean data and with 30-minute data. $g_{c,PM}$ based on 30-minute values was despiked to remove obviously incorrect values. Despiking was done following (Rogiers et al., 2005) in an adjusted way, where a rolling window of three days was applied on the data to calculate mean and standard deviation and all values larger or smaller three times the standard deviation were removed. In addition, the 30-minute g_c values were restricted to the time period between 10 a.m. and 4 p.m. in order to exclude, on the one hand, periods of limited vegetation activity during the night and, on the other hand, periods in which the assumption of a closed energy balance in the inverted Penman-Monteith equation was frequently violated.

Filtering data by periods without interceptions causes systematic gaps, which may cause systematic bias. To still obtain a continuous time series and avoid systematic biases, the next step was to model g_c for all days using the $g_{c,PM}$ data. This modeling step was only possible for the daily average data and performed inadequate for 30-minute data.

To model $g_{c,modeled}$ from the calculated values for all days, the following equation from Runkle et al. (2014) was used:

$$g_{c,modeled} \equiv \frac{aR_g+b}{1+cVPD}. \quad (3)$$

a, b and c were the best fit variables, global radiation (R_g) and VPD the data in a daily resolution. While Runkle et al. (2014) modeled monthly g_c values with equation 3, this approach aimed to achieve a daily resolution. For this purpose of a daily resolution, a moving window of $\pm$15 days was used and $g_{c,PM}$ values in this window were extracted from D and had a selected minimum of four data points. The constants a, b, and c of equation 3 were then adjusted using the curve_fit function of SciPy (Virtanen et al., 2020). The function uses the Levenberg-Marquardt algorithm (Moré, 1977), which is based on the non-linear least squares method. As a quality measure for the model fitting, the root mean square error (RMSE) was used. $g_{c,modeled}$ data was then filtered for the growing season. To determine the point at which the evaporative cooling capacity of the vegetation was limited by VPD or SWC, g_c and VPD as well as g_c and SWC were scattered against each other. Using a local polynomial regression analysis and nonparametric breakpoint detection, the relationship between g_c and VPD, as well as g_c and SWC, was determined. The regime change in g_c was defined as the global maximum of the regression line. The 95% confidence interval of the regression was determined using bootstrapping (n=1000). If g_c decreases with increasing VPD or SWC, g_c was limited by VPD or SWC. For daily g_c data, $g_{c,modeled}$ was used and for 30-minute g_c data $g_{c,PM}$ was used.

2.6 Seasonal energy flux dynamics

The annual and daily variations of the energy components (R_n, SHF, H, LE) and other environmental variables (e.g., GPP, T_a) were examined visually. The composition of the turbulent energy fluxes was determined by the Bowen ratio (B). B was given as the ratio of H to LE ($B = H/LE$). To reduce the influence of outliers from negative energy fluxes, particularly during winter, the data was aggregated into three-day values. B was calculated for time periods in which R_g is above 20 W m^{-2}.

2.7 Statistical analysis

Generalized least squares (GLS) models (Aitken, 1936) with autoregressive (AR) errors (Cochrane and Orcutt, 1949) of the first order (AR(1)) were used to examine the biotic and abiotic variables influencing daily average LE. GLS was used because eddy covariance fluxes and micrometeorological data are temporally autocorrelated, violating the independence assumption of ordinary least squares. Three models were fitted: one covering the entire period from 1 January 2023 to 31 December 2025, a second model covering the growing season, and a third model covering the non-growing season. To control for seasonal effects, in a first step ordinary least squares (OLS) models were created for all relevant predictors (R_n, GPP, VPD, T_a, WTD, and SWC), except g_c, with only the months as predictors. The residuals of the OLS model were the proportions of the dependent variables that are not explained by seasonal effects, which were used as predictors for the further analysis. For all time windows (entire year, growing season, non-growing season), the data were checked for multicollinearity using the variance inflation factor (VIF), whereby all predictors had to have a VIF value of < 10 (Dormann et al., 2013). In addition, the correlation between all pairs of predictors was checked and a Pearson correlation coefficient (r) of $|r| \leq 0.7$ was required for all parameters (Dormann et al., 2013). g_c was not included in the driver analysis, as it was calculated using the inverted Penman-Monteith

equation, which already included R_n and is derived from LE measurements. Therefore, including g_c in the driver analysis would have introduced statistical circularity.

H and T_s were excluded from the models; the reason for the exclusion was a high level of multicollinearity when H was included and a strong collinearity between T_a and T_s. The detrended predictors were normalized to a mean value of 0 and a standard deviation of 1. Normalization made it possible to compare the effect sizes.

To account for temporal autocorrelation in the residuals, a GLSAR AR(1) was used. The order of AR was chosen based on a partial autocorrelation function (PACF) plot. This GLSAR AR(1) model considered the dependency between two neighboring points in time and assumed that the difference between the predicted and actual values (residuals) was not completely random, but partially influenced by the previous value, which is typical for climate data. In addition, the HC3 covariance matrix correction was used to estimate the standard errors, which ensured that the standard errors were robustly estimated even in the case of heteroscedasticity. The use of HC3 was therefore a conservative estimate of the confidence intervals and *p*-values.

The quality of the model was assessed using the R^2 value and the Durbin-Watson statistic (DW) (Durbin and Watson, 1950, 1951, 1971). Temporal autocorrelation was assumed from a DW < 1.5 or > 2.5, whereas a value of 2 meant that no temporal autocorrelation was present.

Working with mean daily values required the time series to be complete, which in EC virtually always requires filling of gaps created during filtering steps. Assessing drivers on gap-filled data bears the danger of circularity, since data that was filled through models is inherently dependent on the predictors used. We assessed the effect of the gap-filled data on the driver analysis by fitting separate models using different thresholds of the maximum percentage of gap-filled values in each day (between 10% and 100%).

The data processing was done with Python 3 (van Rossum and Drake, 2009), in particular the packages Numpy (Harris et al., 2020), Pandas (The pandas development team, 2025), SciPy (Virtanen et al., 2020), scikit-learn (Pedregosa et al., 2011), statsmodels (Seabold and Perktold), Ruptures (Truong et al., 2020), Matplotlib (Hunter, 2007), and Plotly (Plotly Technologies Inc., 2015) which were used to perform statistics, mathematics and data handling and to create figures.

3 Results

3.1 Energy balance closure

The energy balance for the period from 1 January 2023 to 31 December 2025 was made up of a mean value of 41.2 W m^{-2} for LE, 22.5 W m^{-2} for H, 1 W m^{-2} for SHF, and 82.3 W m^{-2} for R_n. The slope of a linear regression between LE + H and R_n – SHF corresponded to 0.83 for all data (Fig. 1).

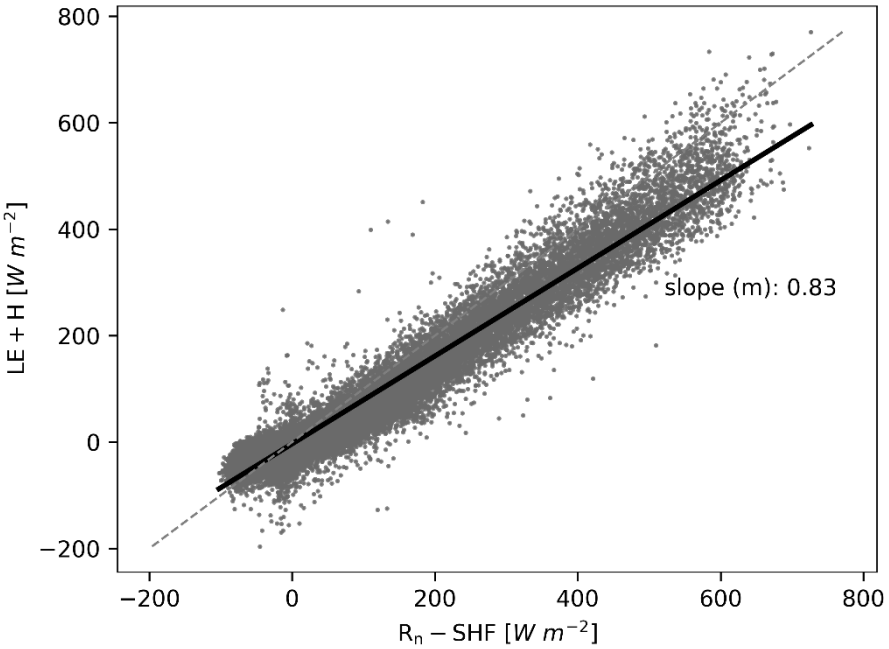


Figure 1: Test of the energy balance closure in DE-Amv during the measurement period (1 January 2023 to 31 December 2025). The x-axis shows the difference of net radiation (Rn) and soil heat flux (SHF). The y-axis shows the mean values for latent heat flux (LE) and sensible energy (H). Values at 30-min resolution are scattered against each other. A linear regression and the slope of the straight line are shown in black, while the dashed gray, dashed line marks the 1:1 relationship.

3.2 Growing seasons

For DE-Amv, in 2023, the growing season began on April 17 and ended on November 8. In 2024, the growing season began on March 24 and ended on October 24. In 2025, the growing season began on April 4 and ended on November 1 (Fig. S3).

3.3 Seasonal energy flux dynamics

The analysis of the monthly average daily fluctuations in the energy flux components showed clear seasonal patterns. H dominated the turbulent energy flux during most months of the first half of the year (from February to May), while LE became the dominant component later in the year (from June to September) (Fig. 2). This seasonal shift of the turbulent energy fluxes was reflected in B, which remained above 1 in the initial months before declining below 1 during June to October in 2023, May to October in 2024, and May to September in 2025 (Fig. 3).

While LE rose in the morning together with R_n, it fell in the afternoon with a delayed response to R_n. VPD and T_a also remained high during early afternoon (Fig. 4). In each month, R_n was the dominant energy component during daytime, while SHF was permanently the lowest. SHF showed a diurnal variation throughout the year, which is delayed in relation to the other energy components.

During the colder months (November to February), turbulent energy fluxes were minimal, with H frequently registering negative values and LE remaining close to zero. Consequently, B also assumed negative values with considerable fluctuations. GPP exhibited a characteristic daily pattern, rising sharply in the morning, peaking before midday, and then gradually declining. This trend mirrored the course of VPD and T_a in an axisymmetric manner. T_s followed a similar pattern to SHF, with minimum values in the morning and an increase towards the evening. Nighttime values of H dropped clearly, reaching the lowest levels in winter. Conversely, LE approached zero at night, with seasonal variations in daily maxima. All four energy flux components (R_n, SHF, H, and LE) displayed steady trends over the year, with smooth transitions between seasonal extremes. The daily peaks of LE and H occurred after those of R_n but preceded SHF maxima.

R_g peaked during June for all years (Figure 5). T_a and VPD peaked between June and August, except for 2024, where VPD had its maximum value in May. SWC was measured at multiple locations, showing consistent trends between locations, despite local heterogeneities. The driest soil conditions were observed in late June and August of 2025, whereas the wettest period occurred during the transitions of the years 2023 and 2024, and 2024 and 2025. P exhibited seasonal variability, with the lowest amount recorded in March 2025 (3 mm $month^{-1}$) and the highest in July 2024 (170.8 mm $month^{-1}$). The by far most intense rainfall event occurred at the 21th of July 2024 (72.2 mm day^{-1}). WTD fluctuated throughout the year, being closer to the surface from January to mid-May before gradually declining until October. Over the three years considered, WTD showed a declining trend.

LE reached its highest values in mid-June to beginning of July. Although general trends were evident, deviations could be observed in all measured variables; for instance, R_g showed frequent high values in early summer (mid-May to June) 2023, which aligned with local maxima in T_a and VPD, coinciding with a drier period marked by low SWC and WTD. Albedo was highest during July and August (a = 0.15 for 2023, a = 0.17 for 2024, and a = 0.13 for 2025) and lowest during December (a = 0.05 for 2023, 0.04 for 2024, and 0.06 for 2025).

Annual P reached 1007 mm y^{-1} in DE-Amv in 2023, 914 mm y^{-1} in 2024, and 562 mm y^{-1} in 2025. 2023, average T_a reached 11.5 °C in DE-Amv. Annual average T_a was 11.6 °C in 2024 and 11 °C in 2025. Mean monthly temperature in DE-Amv was 5.3 °C in January 2023, 3.2 in January 2024, and 2.9 in January 2025 and 17.8 °C in July 2023, 18.3 °C in July 2024, and 18.4 °C in July 2025. SWC ranged from 49% (30th June 2025) to 89% (5th January 2024) (Fig. 5). WTD ranged from –79 cm (30th August 2025) to 0 cm (10th March 2023). T_s reached its minimum at the 20th February 2025at 0.7 °C and its maximum 15th August 2024 at around 23 °C.

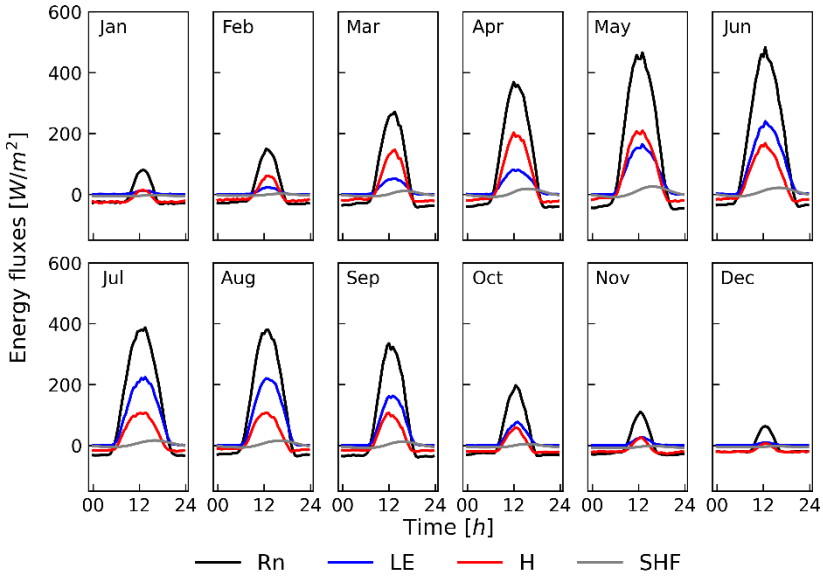


Figure 2: Monthly mean diurnal radiative and turbulent energy fluxes for the measurement period (1 January 2023 to 31 December 2025): In black the net radiation (Rn), in blue the latent heat flux (LE), in red the sensible heat flux (H) and in gray the soil heat flux (SHF). The times indicate the local time of the study site.

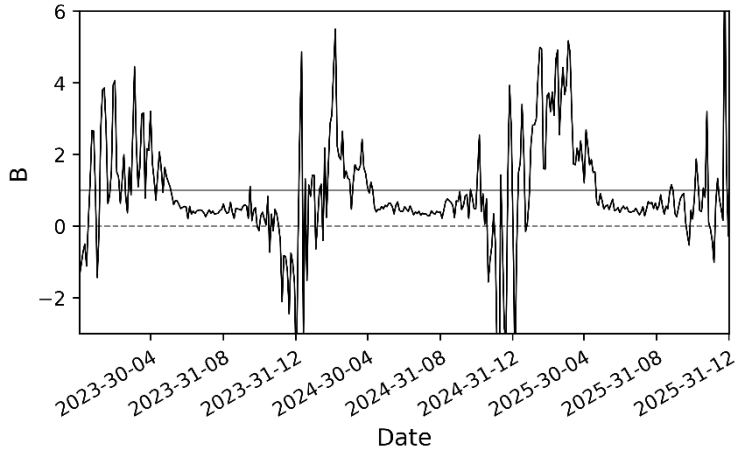
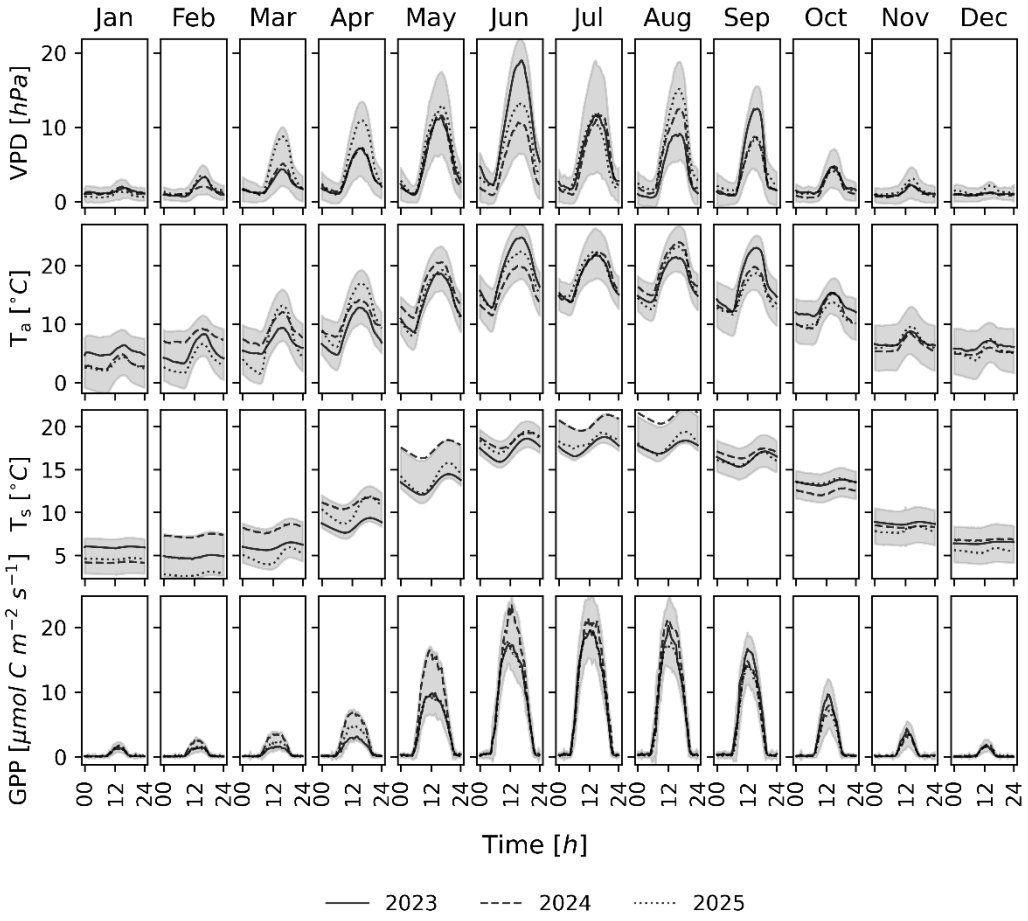
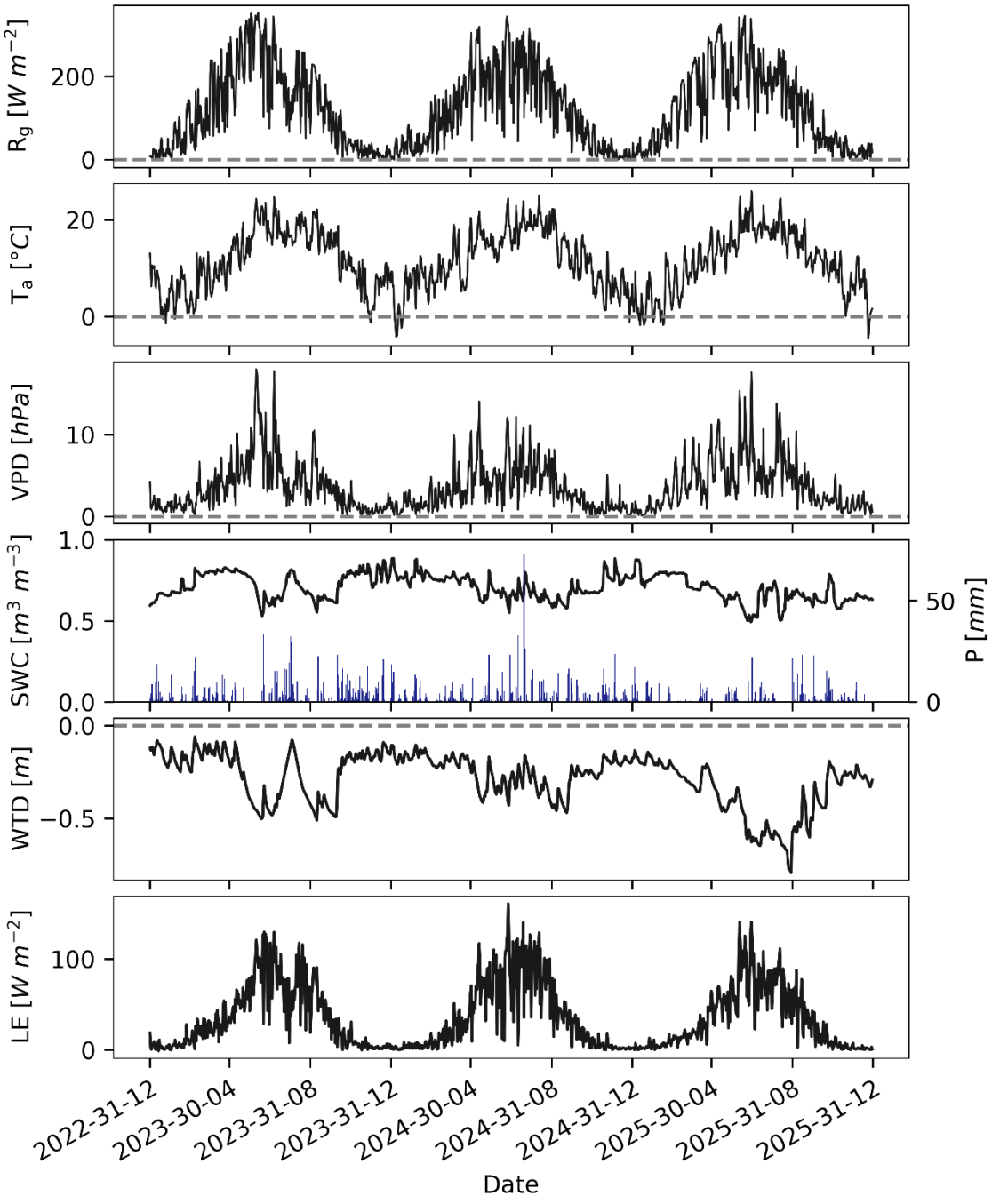


Figure 3: Bowen ratio (B) for the measurement period (1 January 2023 to 31 December 2025): The values are aggregated to three-day values. B values above 1 mean that sensible heat (H) dominates and B values below 1 (vertical solid line) indicate that latent heat flux (LE) assumes larger values than H.



280 **Figure 4: Diurnal patterns by month. The black lines show the mean value by year (solid = 2023, dashed = 2024, dotted = 2025), while the grey area represents the standard deviation of all years (2023, 2024, and 2025) combined. VPD = vapor pressure deficit, Ta = air temperature, Ts = soil temperature, GPP = gross primary production.**



285

Figure 5: Global radiation (Rg), air temperature (Ta), vapor pressure deficit (VPD), soil water content (SWC) at –5 cm depth, in blue the precipitation (P), water table depth (WTD) and latent heat flux (LE) for the measurement period (1 January 2023 to 31 December 2025). The data is displayed at a daily resolution.

3.4 Driver analysis

The GLSAR AR(1) regression results indicated a strong model fit for the entire year and during the growing season. In all trained models VIF values were well below 10 and between the explanatory variables all R values were less than 0.7. The proportion of gap-filled data permitted within daily datapoints had little impact on the driver analysis. Minor effects were observed only when the threshold was reduced to 10%; however, this resulted in substantial data subsampling, rendering the analysis less representative. Both the ranking and the magnitude of all drivers remained consistent across the full range of thresholds for the maximum allowable proportion of gap-filled data per day (Supplementary Fig. S1).

For the entire years 2023 to 2025, the model exhibited a high goodness of fit with an R^2 of 0.811 and an adjusted R^2 of 0.810 (Table 2). The F-statistic of 379.5 ($p < 0.001$) confirmed the overall significance of the model. The DB statistics of 2.076 suggested that temporal autocorrelation had been effectively corrected. During the growing seasons (2023-04-17 to 2023-11-08, 2024-03-24 to 2024-10-24, 2025-04-04 to 2025-11-01), the model fit improved further, with an R^2 of 0.846 and an adjusted R^2 of 0.845. The F-statistic of 410.2 ($p < 0.001$) further confirmed the strong explanatory power of the predictors also in the model for the growing seasons. The DB statistics of 2.041 remained close to the ideal value of 2, indicating near no autocorrelation. In contrast, the non-growing season showed a weaker model fit, with an R^2 of 0.461 and an adjusted R^2 of 0.460. Despite the lower explanatory power, the model remained statistically significant (F-statistic = 40.98, $p < 0.001$). The DB statistics of 2.009 suggested a good level of autocorrelation correction.

In the entire years 2023 to 2025, the standardized residuals of GPP, VPD, R_n, and WTD exhibited significant positive effects on LE, with coefficients of 7.3 for GPP, 7.0 for R_n, 4.6 for VPD, and 2.3 for WTD ($p < 0.001$) (Table 3). SWC showed no significant positive effect on LE, also, T_a has no significant effect on LE. During the growing seasons, all parameters considered, except SWC, showed a significant influence on LE (Table 4). R_n influence on LE was notably stronger compared to the annual results and now has an effect size of 10.3. GPP also gains further weight during the growing season and with 8.5 had a larger effect size than VPD during this time. With a coefficient of 3.9 VPD remained an important predictor, while T_a has a medium positive effect on LE (2.4). During the non-growing season, WTD and VPD had by far the strongest effect, although at 2.5 for WTD and 2.2 for VPD they were weaker than in the previous two time periods (Table 5). GPP also in the non-growing season had a significant effect on LE, although at 1.2 the effect size was small. R_n and T_a almost had no influence on LE. With –1 T_a's effect on LE is negative during the non-growing season. SWC revealed a slightly significant effect during the non-growing season (p=0.042), although the effect size of –0.7 is negligible.

Table 2: Metrics of GLSAR AR(1) models. Data is from 1 January 2023 to 31 December 2025 and the growing season is taking place from 2023-04-17 to 2023-11-08, 2024-03-24 to 2024-10-24, 2025-04-04 to 2025-11-01. DB = Durbin-Watson.

Time frame	R^2	adj. R^2	F-stat.	p (F-stat.)	DB
entire year	0.811	0.810	379.5	< 0.001	2.076
growing season	0.846	0.845	410.2	< 0.001	2.041

non-growing season	0.467	0.460	40.98	< 0.001	2.009

Table 3: Results of GLSAR AR(1) model for the entire years 2023 to 2025. Rn = net radiation, GPP = gross primary production, VPD = vapor pressure deficit, Ta = air temperature, WTD = water table depth, and SWC = soil water content.

Variable of standardized residuals	Coefficient	Standard error	t	*p* > |t|	[0.025	0.975]
R_n	7.0	0.5	15.2	< 0.001	6.1	7.9
GPP	7.3	0.4	17.3	< 0.001	6.5	8.1
VPD	4.6	0.5	9.6	< 0.001	3.7	5.6
T_a	0.1	0.3	0.4	0.714	–0.5	0.8
WTD	2.3	0.5	5.0	< 0.001	1.4	3.2
SWC	–0.7	0.4	–1.8	0.065	–1.4	0.0

Table 4: Results of GLSAR AR(1) model for the growing seasons (2023-04-17 to 2023-11-08, 2024-03-24 to 2024-10-24, 2025-04-04 to 2025-11-01) in 2023 to 2025. Rn = net radiation, GPP = gross primary production, VPD = vapor pressure deficit, Ta = air temperature, WTD = water table depth, and SWC = soil water content.

Variable of standardized residuals	Coefficient	Standard error	t	*p* > |t|	[0.025	0.975]
R_n	10.3	0.7	15.0	< 0.001	8.9	11.6
GPP	8.5	0.6	15.2	< 0.001	7.4	9.6
VPD	3.9	0.7	5.4	< 0.001	2.5	5.3
T_a	2.4	0.6	4.3	< 0.001	1.3	3.5
WTD	2.7	0.6	4.6	< 0.001	1.6	4.0
SWC	–1.0	0.6	–1.6	0.107	–2.3	0.2

Table 5: Results of GLSAR AR(1) model for the non-growing season (2023-01-01 to 2023-04-16 and 2023-11-09 to 2023-12-31, 2024-01-01 to 2024-03-23 and 2024-10-25 to 2024-12-31, 2025-01-01 to 2025-04-03 and 2025-11-02 to 2025-12-31) 2023 to 2025. Rn = net radiation, GPP = gross primary production, VPD = vapor pressure deficit, Ta = air temperature, WTD = water table depth, and SWC = soil water content.

Variable of standardized residuals	Coefficient	Standard error	t	*p* > |t|	[0.025	0.975]
R_n	1.7	0.2	7.2	< 0.001	1.2	2.2
GPP	1.2	0.2	5.7	< 0.001	0.8	1.7

VPD	2.2	0.3	7.6	< 0.001	1.6	2.7
T_a	–1.0	0.3	–3.2	0.001	–1.6	–0.4
WTD	2.5	0.5	4.7	< 0.001	1.4	3.5
SWC	–0.7	0.3	–2.0	0.042	–1.4	–0.03

330

3.5 Canopy conductance

3.5.1 Daily canopy conductance

The results of $g_{c,modeled}$ are daily values calculated down to mm s^{-1} and accordingly show the mean value for the individual days. $g_{c,modeled}$ shows some gaps, which are due to a lack of data points from $g_{c,PM}$(Fig. 6). With peaks above 20 mm s^{-1}, $gc_{,modeled}$ was highest in August 2024 (Fig. 6). In 2023 as well, $g_{c,modeled}$ peaked in August, while in 2025 a decline in $g_{c,modeled}$ can be observed during that period. Although $g_{c,modeled}$ peak was lowest in 2025, it was the most stable year regarding peak season. All three years under consideration – 2023, 2024, and 2025 – exhibited a clear seasonal pattern in which $g_{c,modeled}$ increased exponentially at the beginning of the growing season, peaked around August, but also increased in variance and maintained this variance toward the end of the growing season, while $g_{c,modeled}$ declined again. $g_{c,modeled}$ values were filtered for the growing seasons (2023-04-17 to 2023-11-08, 2024-03-24 to 2024-10-24, 2025-04-04 to 2025-11-01), as active vegetation could be assumed during this period. $g_{c,modeled}$ was close to 0 in the omitted periods except around January 2025.

$g_{c,modeled}$ was used to analyze the relationship between g_c and VPD, and g_c and SWC to better understand the role of vegetation (Fig. 7, Fig. 8). For VPD, a local polynomial regression suggested a maximum $g_{c,modeled}$ (8.9 mm s^{-1}) at around 4.6 hPa VPD before gradually declining at higher VPD (Fig. 7). Mean values of $g_{c,modeled}$ decreased after this threshold of 4.6 hPa VPD. Below the aforementioned VPD threshold, the regression showed a positive correlation between VPD and $g_{c,modeled}$; at the same time, the 95% confidence interval of the regression line widened substantially and a noticeable increase in standard deviation for $g_{c,modeled}$ was observed as VPD decreased.

For SWC, $g_{c,modeled}$ increased with SWC until SWC reached 65% (Fig. 8). After this threshold, $g_{c,modeled}$ decreased as SWC increased, and the decrease was more pronounced than the increase that occurred before the threshold as SWC increased. As was also observed for atmospheric dryness (VPD), the standard deviation of $g_{c,modeled}$ decreased as soil dryness increased (SWC decreased).

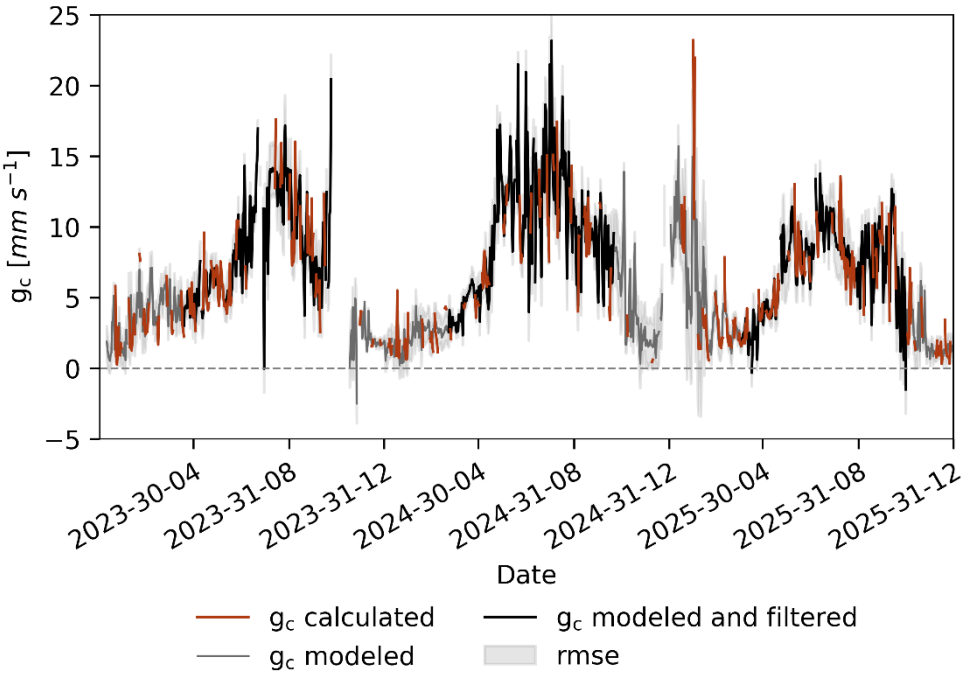


Figure 6: Canopy conductance (gc) and root mean square error (RMSE) in mm s–1. In red values calculated with equation 2, in gray gc values modeled with equation 3, in black the modeled values after filtering and the RMSE of the modeled data in light gray. The values are calculated on a daily basis.

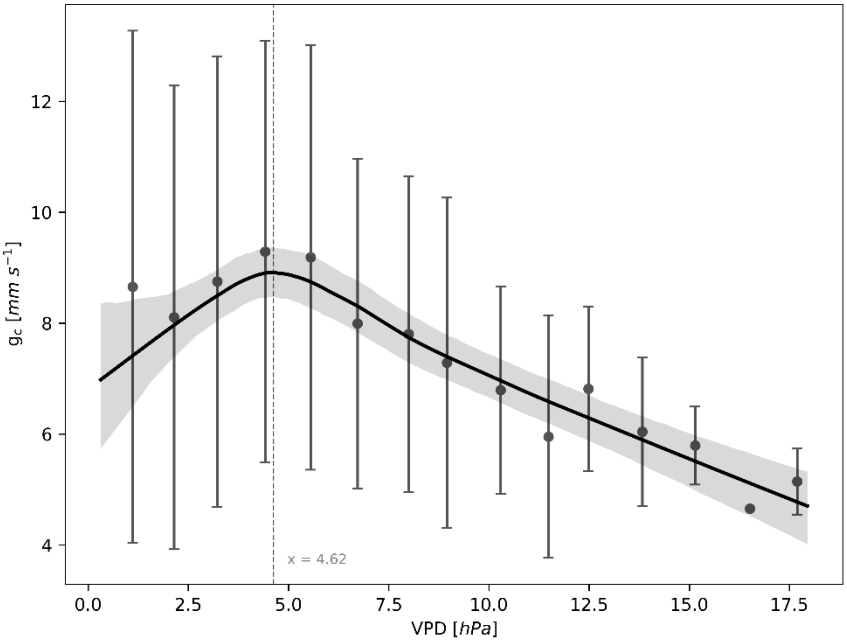


Figure 7: Relationship between modeled canopy conductance (gc,modeled) and vapor pressure deficit (VPD). The data are daily averages for gc,modeled using equation 3. Vertical solid lines in gray show mean and standard deviation for bins of the individual data points, in black a local polynomial regression. Gray area shows the 95% confidence interval of the regression obtained using bootstrapping (n=1000). The vertical dashed line indicates the maximum of the regression line. Data were restricted to the growing seasons.

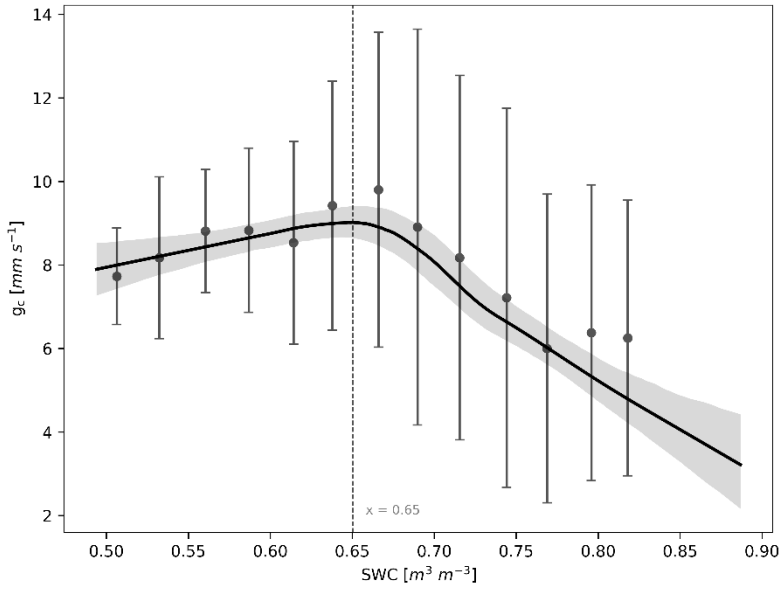


Figure 8: Relationship between modeled canopy conductance (gc,modeled) and soil water content (SWC). The data are daily averages for gc,modeled using equation 3. Vertical lines in gray show mean and standard deviation for bins of the individual data points, in black a local polynomial regression. Gray area shows the 95% confidence interval of the regression obtained using bootstrapping (n=1000). The vertical dashed line indicates the maximum of the regression line. Data were restricted to the growing seasons.

3.5.2 30-minute canopy conductance

$g_{c,PM}$ reached its highest daily maximum in July and August, while the smallest daily variations with the lowest maximum values were observed in April and May (Fig. 9). The 30-minute $g_{c,PM}$ time series contained several outliers whose pronounced intensity obscured weaker outliers for the filter; nevertheless, a clear diurnal cycle is evident for all months, particularly from June through October. $g_{c,PM}$ rose until around 11:00 and then declined continuously, with the peak occurring earlier in April and May and at around 12:00, later in June.

For the 30-minute data, the regression analysis revealed a maximum in $g_{c,PM}$ at a VPD of 7.6 hPa (Fig. 10). Below the threshold of 7.6 hPa VPD, $g_{c,PM}$ increased with VPD, accompanied by a pronounced standard deviation. Above the threshold, $g_{c,PM}$ decreased as VPD increased, and the standard deviation also decreased as VPD increased. For $g_{c,PM}$ and SWC, a threshold of 0.62% SWC was observed (Fig. 11). For values above this threshold of 0.62% SWC, a decrease in $g_{c,PM}$ was apparent with increasing SWC, whereas below the threshold, there was no significant correlation between $g_{c,PM}$ and SWC according to the 95% confidence interval of the regression line. The standard deviation of $g_{c,PM}$ showed no trend for SWC.

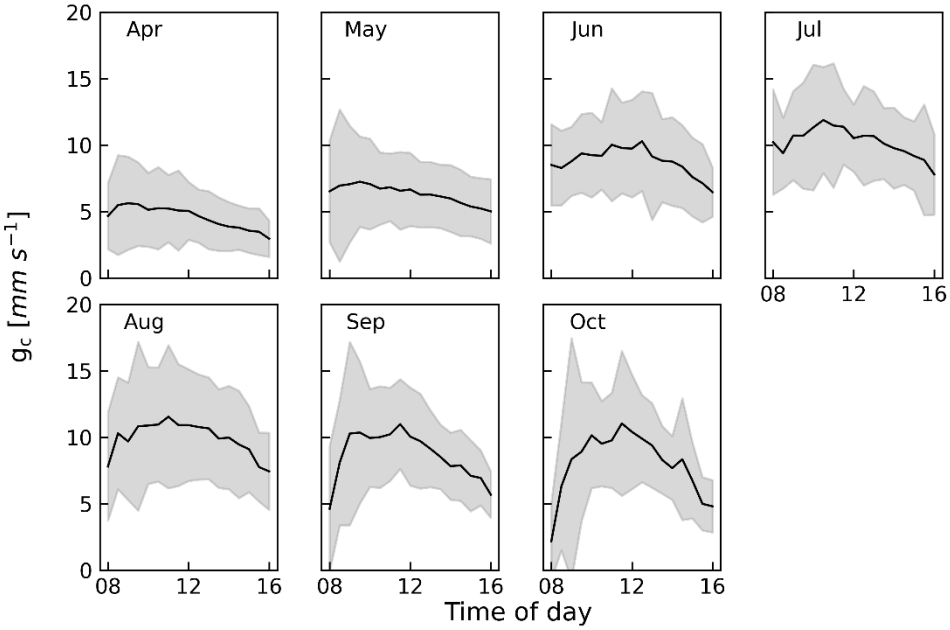


Figure 9: Diurnal patterns by month. The black line shows mean canopy conductance calculated using equation 2 (gc,PM) and the gray area shows its standard deviation. Data was restricted to the growing seasons.

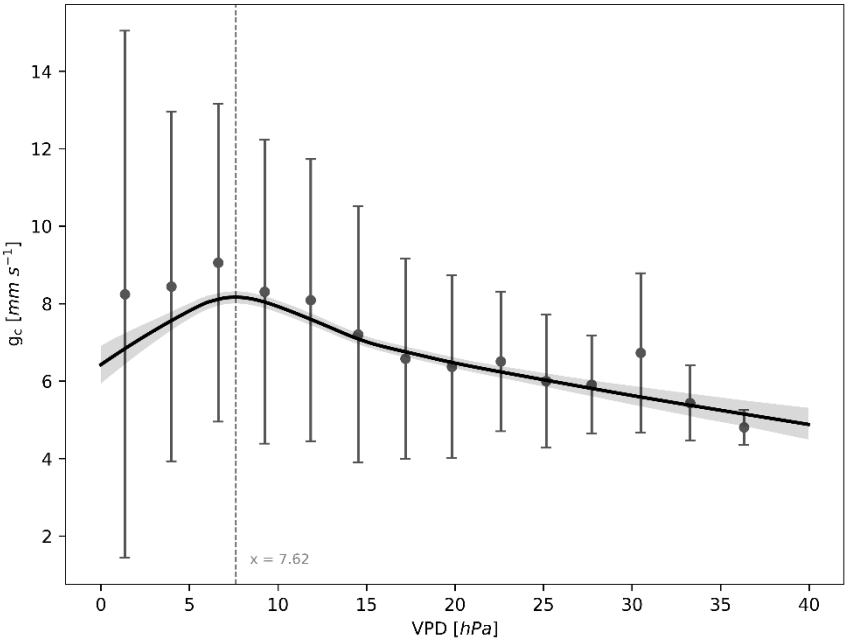


Figure 10: Relationship between calculated canopy conductance (gc,PM) and vapor pressure deficit (VPD). The data have a resolution of 30-minutes and were calculated using equation 2. Vertical lines in gray show mean and standard deviation for bins of the individual data points, in black a local polynomial regression. Gray area shows the 95% confidence interval of the regression obtained using bootstrapping (n=1000). The vertical dashed line indicates the maximum of the regression line. Data were restricted to the growing seasons and between 8h and 16h.

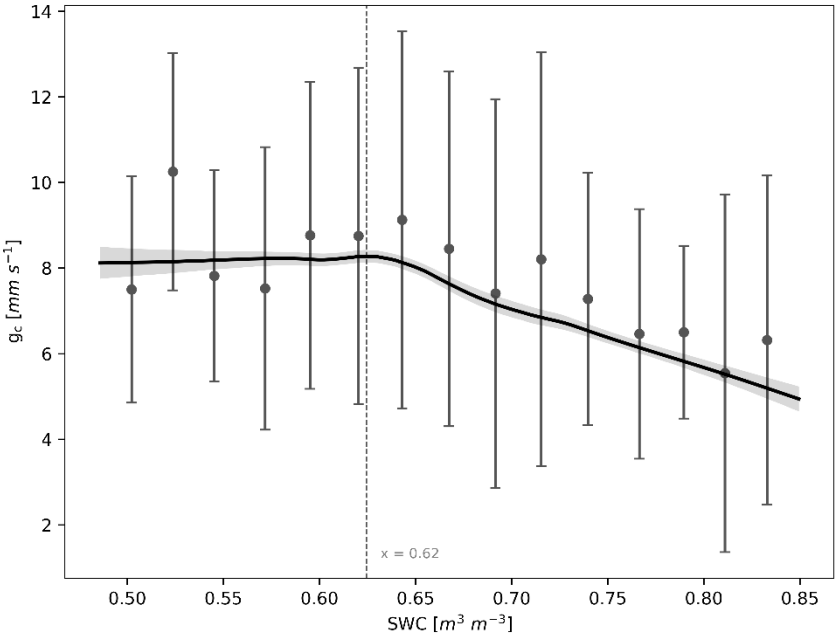


Figure 11: Relationship between calculated canopy conductance ($g_{c,PM}$) and soil water content (SWC). The data have a resolution of 30-minutes and were calculated using equation 2. Vertical lines in gray show mean and standard deviation for bins of the individual data points, in black a local polynomial regression. Gray area shows the 95% confidence interval of the regression obtained using bootstrapping (n=1000). The vertical dashed line indicates the maximum of the regression line. Data were restricted to the growing seasons and between 8h and 16h.

4 Discussion

4.1 Energy balance closure and data quality

This study provides the first analysis of biotic and abiotic drivers of LE fluxes in a peatland of the Central European lowlands. The energy balance closure was 83%, which falls within the typical range reported for the EC method (70-90%; Twine et al., 2000) and is above average for wetlands which is in average around 77% (Nicolini et al., 2026). In our experimental setup, part of the residual imbalance likely arose from several well-known limitations of the EC method (Mauder et al., 2024). In peatland environments, advective transport of heat and water can represent a non-negligible component of the energy balance residual. In addition, large turbulent eddies with time scales exceeding the EC averaging period may contribute to the imbalance, as these motions are not fully captured by standard flux calculations. Further sources of imbalance include low pass filtering of water vapor by the intake tube of the gas analyzer, general measurement uncertainties, unaccounted energy storage (e.g., in soil or biomass), and errors introduced during data processing (Mauder et al., 2024; Nicolini et al., 2026).

Despite these limitations, the observed closure indicates that the energy flux measurements are of sufficient quality to support robust analysis and interpretation.

4.2 Temporal dynamics of latent heat flux

When comparing turbulent energy fluxes in DE-Amv with similar sites (e.g., Gerling et al., 2019), during the warm season, LE generally dominates H, regardless of the site and its local climate. Gerling et al. (2019) found Bowen ratios < 1 in a central European mountainous peatland in July and August, similar to Gunawardhana et al. (2021) in an Australian peatland and Runkle et al. (2014) in a boreal peatland, where LE was several times higher than H. In the cold season, particularly in spring, B varies across regions: Alekseychik et al. (2017) and Runkle et al. (2014) observed LE > H during all measured months in boreal peatlands, while Gunawardhana et al. (2021) found B > 1 in Australian mountains, as in DE-Amv. In fall, the mountain valley bog in Australia had B < 1, whereas in DE-Amv, LE continued to exceed H. One possible explanation is that available energy goes more into LE than into H and that this ratio only reverses when LE is limited. Mamadou et al. (2016), for example, identified water availability in the soil as the main driver for changes in the Bowen ratio, whereby they investigated two different areas (cultivated area and woodland) in Northern Benin, where a dry and a rainy season exist. However, further research is needed to be able to make reliable statements about the underlying causes of the interaction between LE and H, particularly in the considered context of peatlands.

4.3 Drivers of latent heat flux

The GLSAR model enabled us to disentangle the individual effects on LE, which could not be achieved using correlation coefficients alone. The strong multicollinearity observed in the correlation analysis was largely driven by the seasonal co-variation with R_g. This issue was effectively mitigated through residualization, allowing for a more reliable assessment of biotic and abiotic drivers.

R_n serves as primary energy source for LE and influences it through two main mechanisms. First, it drives surface evaporation e.g., from soil. Second, it provides the energy necessary for biological activity, enabling vegetation to transpire and thereby further enhance LE. The pronounced influence of R_n on LE during the growing season likely reflects this overarching role. Outside the growing season, however, the residual aboveground vegetation in DE-Amv continues to shade the soil, limiting the direct impact of R_n on surface evaporation. Here, we decided to remove the diurnal variations and the average seasonality of the years from the driver analysis in order to reduce the multicollinearity among the explanatory variables, but also because we are interested in the variable component of R_n. It is not surprising that R_n provides the energy for ecological processes. The mean seasonality can vary with three years of data, which may influence the effect size of R_n on LE. Additionally, different approaches to detrending can influence the effect size of R_n on LE as well.

Although higher VPD physically promotes faster water evaporation, vegetation can counteract this through stomatal closure to prevent desiccation (Grossiord et al., 2020). Nevertheless, this physical relationship helps explain why VPD shows a strong influence on LE, particularly outside the growing season when stomatal regulation is largely absent. With global VPD expected

to rise under climate change (Shekhar et al., 2024; Yuan et al., 2019), LE in DE-Amv is likely to be affected. Increases in VPD can enhance LE up to the point at which stomatal regulation limits transpiration, potentially offsetting or reversing this effect. While stomatal control has been well-documented in forest ecosystems under variable environmental conditions, our results – consistent with a limited number of studies – indicate that this mechanism also plays a significant role in peatland ecosystems. The effect of stomatal control is not only evident in 30-minute data but also remains clearly pronounced in daily average data. This indicates that vegetation is limited not only for brief periods during the day but in principle by atmospheric dryness. Consequently, the presence and variability of stomatal regulation across sites and vegetation types should be carefully considered in models of ecosystem energy, carbon, and water fluxes.

The absence of a g_c limitation for decreases in 30-minute SWC indicates that soil dryness does not limit transpiration in DE-Amv. Furthermore, the driver analysis also revealed no effect of SWC on LE. These findings are consistent with previous research, which identified VPD as the dominant driver of LE and g_c for areas with higher water availability (Zhang et al., 2024; Fu et al., 2022), such as peatlands. In contrast, compared to VPD, SWC dominates the limitation of LE in areas where water is limited (Zhang et al., 2024) and can contribute to intensifying heat extremes (Hirschi et al., 2011). Against this background, the results of this study highlight the importance of wetland ecosystems, their conservation, and their restoration. With 2023 and 2024, data includes the two years with highest and third-highest annual P since 2007, followed by the second-lowest annual P (2025) since 2007 (DWD, 2022). The lack of LE limitations due to soil dryness despite the dry year of 2025 may be due to continued sufficient soil moisture but could also potentially be attributed to legacy effects from the preceding wet years (Du et al., 2024). Three years of data limit conclusions regarding changes in LE driver effect sizes during or after extreme events, even though the 95% confidence intervals of the driver analysis are sufficiently narrow to provide robust results.

While meteorological factors such as R_n and VPD are frequently identified as the main drivers of LE (e.g., Gunawardhana et al. (2021) in a mountainous peatland), GPP is less often reported as a dominant driver. For example, Eichelmann et al. (2022) found that vegetation contributed 70 – 75% to LE in California wetlands, and in this study as well, GPP, along with R_n, was the most important driver of LE. This discrepancy likely reflects the greater heterogeneity of vegetation compared to meteorological factors, both spatially and temporally. Furthermore, GPP is challenging to predict for the future: although it is expected to increase under climate change (Lu et al., 2024), the anticipated rise in extreme events, such as droughts, can alter the water balance and consequently GPP (Beniston et al., 2007). Therefore, further research is needed to understand how extreme events may modify the relative influence of different drivers on LE.

As the non-growing season is characterized by very low LE fluxes, very small influences such as that of T_a may not be statistically interpretable. Nevertheless, the effect size of VPD and WTD residuals are sufficiently strong (coefficients: VPD = 2.2, WTD = 2.5) to assume a genuine correlation between VPD and LE, as well as WTD and LE during the non-growing season.

g_c peaked in summer, suggesting a delayed response of g_c to increasing VPD. The relationship between g_c and VPD observed here does not follow the exponential pattern reported in other studies (Runkle et al., 2014; Xu et al., 2021). This deviation may result from high variability in g_c among species, leaf age, and environmental conditions (Song et al., 2022; Xu et al., 2021).

For instance, Gobin et al. (2015) observed that *Calluna vulgaris* did not significantly close stomata under increasing VPD when soils were saturated, with similar results for *Molinia caerulea*, albeit at lower transpiration rates.

4.4 Limitations of the modeled canopy conductance

While g_c based on daily averages has made it possible to create a g_c time series with only few outliers and no bias caused by exclusively rain-free days, there are still limitations compared to 30-minute g_c calculations. Averaging to daily values results in loss of information regarding the diurnal cycle; however, this cycle is pronounced in VPD and is therefore potentially important for g_c as well. Furthermore, averaging input variables in nonlinear functions, such as the Penman-Monteith equation and equation 3, can introduce Jensen-type biases because model outputs calculated from averaged inputs generally differ from averages of high-temporal-resolution outputs (Denny, 2017). Jensen's inequality can be avoided by using unaveraged 30-minute values, although this results in more outliers, which can be explained by missing energy storage terms. For example, the standard deviation in April and May is noticeably greater in the mornings compared to later the day, which can be explained, among other storage terms, by soil heating above the SHF sensors (Nicolini et al., 2026). The fact that both approaches – averaged and unaveraged g_c – show no unexpected differences from one another nevertheless speaks to the robustness of the approach.

5 Conclusion

This study demonstrates that LE in Central European drained bogs is primarily driven by a combination of R_n and GPP, with atmospheric demand (VPD) playing a crucial role, especially outside the growing season. The finding that stomatal regulation significantly limits transpiration – even in water abundant peatlands – highlights that these ecosystems are more biologically controlled than previously assumed in simple energy driven models of LE. While the three-year dataset provides robust insights, longer-term monitoring is required to understand how extreme climatic events modify the relative influence of the identified drivers.

DE-Amv is planned for rewetting in the near future, which could alter peatland water balance, vegetation composition, canopy structure, and leaf area, thereby affecting LE. For example, if *Molinia caerulea*, which tolerates higher moisture, expands, LE could decrease (Gobin et al., 2015), while its sensitivity to VPD might remain unchanged. A more detailed evaluation of the contributions of individual functional plant groups – potentially by linking g_c with phenological patterns – will be crucial for accurately predicting future LE dynamics and understanding the role of peatland ecosystems in regulating climate through energy fluxes. Overall, our results highlight that vegetation plays a significant and dynamic role in controlling LE in peatland ecosystems. Accurately accounting for species composition, functional traits, and stomatal regulation will be essential for predicting future LE dynamics and for understanding the contribution of peatlands to regional and global climate regulation.

Declaration of generative AI and AI-assisted technologies in the writing process

During the preparation of this work the author(s) used deepl.com in order to help with the translation from German into English. After using this tool/service, the author(s) reviewed and edited the content as needed and take(s) full responsibility for the content of the published article.

Code availability statement

Code is available upon request.

Data availability statement

Eddy covariance and micrometeorological data are available via ICOS Carbon Portal under doi.org/10.18160/S6HM-CP8Q.

Declaration of competing interest

The authors declare no conflict of interest.

Author contribution

VF: formal analysis, methodology, software, visualization, writing (original draft preparation), writing (review and editing). NB: data curation, formal analysis, methodology, supervision, validation, writing (review and editing). MG: conceptualization, funding acquisition, methodology, project administration, resources, supervision, validation, writing (review and editing).

References

Aitken, A. C.: IV.—On Least Squares and Linear Combination of Observations, Proc. R. Soc. Edinb., 55, 42–48, doi:10.1017/S0370164600014346, 1936.

Alekseychik, P., Mammarella, I., Karpov, D., Dengel, S., Terentieva, I., Sabrekov, A., Glagolev, M., and Lapshina, E.: Net ecosystem exchange and energy fluxes measured with the eddy covariance technique in a western Siberian bog, Atmos. Chem. Phys., 17, 9333–9345, doi:10.5194/acp-17-9333-2017, 2017.

Beck, P. S., Atzberger, C., Høgda, K. A., Johansen, B., and Skidmore, A. K.: Improved monitoring of vegetation dynamics at very high latitudes: A new method using MODIS NDVI, Remote Sensing of Environment, 100, 321–334, doi:10.1016/j.rse.2005.10.021, 2006.

Beniston, M., Stephenson, D. B., Christensen, O. B., Ferro, C. A. T., Frei, C., Goyette, S., Halsnaes, K., Holt, T., Jylhä, K., Koffi, B., Palutikof, J., Schöll, R., Semmler, T., and Woth, K.: Future extreme

events in European climate: an exploration of regional climate model projections, Climatic Change, 81, 71–95, doi:10.1007/s10584-006-9226-z, 2007.
Chen, T. and Guestrin, C.: XGBoost, Machinery, New York, USA, 785–794, doi:10.1145/2939672.2939785, 2016.
Climate Data Center: https://cdc.dwd.de/portal/202209231028/view1, last access: 12 April 2024.
Cochrane, D. and Orcutt, G. H.: Application of Least Squares Regression to Relationships Containing Auto-Correlated Error Terms, Journal of the American Statistical Association, 44, 32–61, doi:10.1080/01621459.1949.10483290, 1949.
Collaborative data science: https://plot.ly.
Denny, M.: The fallacy of the average: on the ubiquity, utility and continuing novelty of Jensen's inequality, The Journal of experimental biology, 220, 139–146, doi:10.1242/jeb.140368, 2017.
Dingman, S. L.: Physical hydrology, Third edition, Waveland Press Inc, Long Grove, Illinois, 643 pp., 2015.
Dormann, C. F., Elith, J., Bacher, S., Buchmann, C., Carl, G., Carré, G., Marquéz, J. R. G., Gruber, B., Lafourcade, B., Leitão, P. J., Münkemüller, T., McClean, C., Osborne, P. E., Reineking, B., Schröder, B., Skidmore, A. K., Zurell, D., and Lautenbach, S.: Collinearity: a review of methods to deal with it and a simulation study evaluating their performance, Ecography, 36, 27–46, doi:10.1111/j.1600-0587.2012.07348.x, 2013.
Du, Q., Guan, Q., Sun, Y., Wang, Q., Zhang, J., Xiao, X., Liu, H., Yang, X., and Zhang, E.: Legacy effects of extreme drought and wetness events on mountain grassland ecosystems and their elevation dependence, Journal of Hydrology, 630, 130757, doi:10.1016/j.jhydrol.2024.130757, 2024.
Durbin, J. and Watson, G. S.: Testing for Serial Correlation in Least Squares Regression: I, Biometrika, 37, 409, doi:10.2307/2332391, 1950.
Durbin, J. and Watson, G. S.: Testing for Serial Correlation in Least Squares Regression. II, Biometrika, 38, 159–178, doi:10.1093/biomet/38.1-2.159, 1951.
Durbin, J. and Watson, G. S.: Testing for Serial Correlation in Least Squares Regression. III, Biometrika, 58, 1, doi:10.2307/2334313, 1971.
Eichelmann, E., Mantoani, M. C., Chamberlain, S. D., Hemes, K. S., Oikawa, P. Y., Szutu, D., Valach, A., Verfaillie, J., and Baldocchi, D. D.: A novel approach to partitioning evapotranspiration into evaporation and transpiration in flooded ecosystems, Global change biology, 28, 990–1007, doi:10.1111/gcb.15974, 2022.
Europäische Union: Standard-Datenbogen: DE3807301, in: Natura 2000-Gebiete in Nordrhein-Westfalen - Fachinformation - Listen der Natura 2000-Gebiete, Landesamt für Natur, Umwelt und Verbraucherschutz Nordrhein-Westfalen (Ed.), 2021.
Fay, E. and Lavoie, C.: The impact of birch seedlings on evapotranspiration from a mined peatland: an experimental study in southern Quebec, Canada, Mires and Peat, 5, 2009.
Fu, Z., Ciais, P., Prentice, I. C., Gentine, P., Makowski, D., Bastos, A., Luo, X., Green, J. K., Stoy, P. C., Yang, H., and Hajima, T.: Atmospheric dryness reduces photosynthesis along a large range of soil water deficits, Nature communications, 13, 989, doi:10.1038/s41467-022-28652-7, 2022.
Gerling, L., Weber, T. K., Reineke, D., Durner, W., Martin, S., and Weber, S.: Eddy covariance based surface-atmosphere exchange and crop coefficient determination in a mountainous peatland, Ecohydrology, 12, doi:10.1002/eco.2047, 2019.

Gharun, M., Hörtnagl, L., Paul-Limoges, E., Ghiasi, S., Feigenwinter, I., Burri, S., Marquardt, K., Etzold, S., Zweifel, R., Eugster, W., and Buchmann, N.: Physiological response of Swiss ecosystems to 2018 drought across plant types and elevation, Philosophical transactions of the Royal Society of London. Series B, Biological sciences, 375, 20190521, doi:10.1098/rstb.2019.0521, 2020.

Gobin, R., Korboulewsky, N., Dumas, Y., and Balandier, P.: Transpiration of four common understorey plant species according to drought intensity in temperate forests, Annals of Forest Science, 72, 1053–1064, doi:10.1007/s13595-015-0510-9, 2015.

Grossiord, C., Buckley, T. N., Cernusak, L. A., Novick, K. A., Poulter, B., Siegwolf, R. T. W., Sperry, J. S., and McDowell, N. G.: Plant responses to rising vapor pressure deficit, The New phytologist, 226, 1550–1566, doi:10.1111/nph.16485, 2020.

Gunawardhana, M., Silvester, E., Jones, O. A., and Grover, S.: Evapotranspiration and biogeochemical regulation in a mountain peatland: insights from eddy covariance and ionic balance measurements, Journal of Hydrology: Regional Studies, 36, 100851, doi:10.1016/j.ejrh.2021.100851, 2021.

Harris, C. R., Millman, K. J., van der Walt, S. J., Gommers, R., Virtanen, P., Cournapeau, D., Wieser, E., Taylor, J., Berg, S., Smith, N. J., Kern, R., Picus, M., Hoyer, S., van Kerkwijk, M. H., Brett, M., Haldane, A., Del Río, J. F., Wiebe, M., Peterson, P., Gérard-Marchant, P., Sheppard, K., Reddy, T., Weckesser, W., Abbasi, H., Gohlke, C., and Oliphant, T. E.: Array programming with NumPy, Nature, 585, 357–362, doi:10.1038/s41586-020-2649-2, 2020.

Heijmans, M. M. P. D., van der Knaap, Y. A. M., Holmgren, M., and Limpens, J.: Persistent versus transient tree encroachment of temperate peat bogs: effects of climate warming and drought events, Global change biology, 19, 2240–2250, doi:10.1111/gcb.12202, 2013.

Hirschi, M., Seneviratne, S. I., Alexandrov, V., Boberg, F., Boroneant, C., Christensen, O. B., Formayer, H., Orlowsky, B., and Stepanek, P.: Observational evidence for soil-moisture impact on hot extremes in southeastern Europe, Nature Geosci, 4, 17–21, doi:10.1038/ngeo1032, 2011.

Humphreys, E. R., Lafleur, P. M., Flanagan, L. B., Hedstrom, N., Syed, K. H., Glenn, A. J., and Granger, R.: Summer carbon dioxide and water vapor fluxes across a range of northern peatlands, J. Geophys. Res., 111, doi:10.1029/2005JG000111, 2006.

Hunter, J. D.: Matplotlib: A 2D Graphics Environment, Comput. Sci. Eng., 9, 90–95, doi:10.1109/MCSE.2007.55, 2007.

Karimi, S., Maher Hasselquist, E., Salimi, S., Järveoja, J., and Laudon, H.: Rewetting impact on the hydrological function of a drained peatland in the boreal landscape, Journal of Hydrology, 641, 131729, doi:10.1016/j.jhydrol.2024.131729, 2024.

Kettridge, N. and Waddington, J. M.: Towards quantifying the negative feedback regulation of peatland evaporation to drought, Hydrological Processes, 28, 3728–3740, doi:10.1002/hyp.9898, 2014.

Kottek, M., Grieser, J., Beck, C., Rudolf, B., and Rubel, F.: World Map of the Köppen-Geiger climate classification updated, metz, 15, 259–263, doi:10.1127/0941-2948/2006/0130, 2006.

Lafleur, P. M., Hember, R. A., Admiral, S. W., and Roulet, N. T.: Annual and seasonal variability in evapotranspiration and water table at a shrub-covered bog in southern Ontario, Canada, Hydrological Processes, 19, 3533–3550, doi:10.1002/hyp.5842, 2005.

Limpens, J., Holmgren, M., Jacobs, C. M. J., van der Zee, S. E. A. T. M., Karofeld, E., and Berendse, F.: How does tree density affect water loss of peatlands? A mesocosm experiment, PloS one, 9, e91748, doi:10.1371/journal.pone.0091748, 2014.

Liu, H., Rezanezhad, F., and Lennartz, B.: Impact of land management on available water capacity and water storage of peatlands, Geoderma, 406, 115521, doi:10.1016/j.geoderma.2021.115521, 2022.

Loescher, H. W., Hanson, C. V., and Ocheltree, T. W.: The Psychrometric Constant Is Not Constant: A Novel Approach to Enhance the Accuracy and Precision of Latent Energy Fluxes through Automated Water Vapor Calibrations, Journal of Hydrometeorology, 10, 1271–1284, doi:10.1175/2009JHM1148.1, 2009.

Lu, Q., Liu, H., Wei, L., Zhong, Y., and Zhou, Z.: Global prediction of gross primary productivity under future climate change, The Science of the total environment, 912, 169239, doi:10.1016/j.scitotenv.2023.169239, 2024.

Mamadou, O., Galle, S., Cohard, J.-M., Peugeot, C., Kounouhewa, B., Biron, R., Hector, B., and Zannou, A. B.: Dynamics of water vapor and energy exchanges above two contrasting Sudanian climate ecosystems in Northern Benin (West Africa), JGR Atmospheres, 121, doi:10.1002/2016JD024749, 2016.

Massmann, A., Gentine, P., and Lin, C.: When Does Vapor Pressure Deficit Drive or Reduce Evapotranspiration?, Journal of advances in modeling earth systems, 11, 3305–3320, doi:10.1029/2019MS001790, 2019.

Matos, K. A., Bowen, G. J., Good, S. P., and Allen, S. T.: Evapotranspiration Partitioning Across US Ecoregions: A Multi-Site Study Using Field Stable-Isotope Observations, Geophysical Research Letters, 52, doi:10.1029/2025gl115367, 2025.

Mauder, M., Jung, M., Stoy, P., Nelson, J., and Wanner, L.: Energy balance closure at FLUXNET sites revisited, Agricultural and Forest Meteorology, 358, 110235, doi:10.1016/j.agrformet.2024.110235, 2024.

Miralles, D. G., Vilà-Guerau de Arellano, J., McVicar, T. R., and Mahecha, M. D.: Vegetation-climate feedbacks across scales, Annals of the New York Academy of Sciences, 1544, 27–41, doi:10.1111/nyas.15286, 2025.

Moore, P. A., Pypker, T. G., and Waddington, J. M.: Effect of long-term water table manipulation on peatland evapotranspiration, Agricultural and Forest Meteorology, 178-179, 106–119, doi:10.1016/j.agrformet.2013.04.013, 2013.

Moré, J. J.: The Levenberg-Marquardt algorithm: Implementation and theory, 1977.

Morgan, B. E., Araki, R., Trugman, A. T., and Caylor, K. K.: Ecological and hydroclimatic determinants of vegetation water-use strategies, Nature ecology & evolution, 9, 1791–1799, doi:10.1038/s41559-025-02810-8, 2025.

Natura 2000: https://environment.ec.europa.eu/topics/nature-and-biodiversity/natura-2000_en.

Nicolini, G., Durden, D., Di Fiore, L., Florian, C., Sabbatini, S., Gielen, B., Iserbyt, A., Loubet, B., Mammarella, I., Mariotti, A., Beeck, M. op de, Slemmons, C., Trotta, C., Young, A., Chabbi, A., Feigenwinter, I., Heinesch, B., Kowalska, N., Mauder, M., Šigut, L., van der Molen, M., Bastos Campos, F., Berveiller, D., Brümmer, C., Cuntz, M., Domec, J.-C., Dumont, B., Fares, S., Gianelle, D., Jensen, R., Kalalian, C., Kljun, N., Lange, H., Limousin, J.-M., Lundin, E., Manco, A., Montagnani, L., Nemitz, E., Peichl, M., Rinne, E., Roland, M., Schmidt, M., Simioni, G., Thomas, A., Vincke, C., and Papale, D.: Bridging the Energy Balance Gap in Eddy-Covariance Measurements: Insights From Standardized Network Data, Global change biology, 32, e70892, doi:10.1111/gcb.70892, 2026.

Nijp, J. J., Metselaar, K., Limpens, J., Teutschbein, C., Peichl, M., Nilsson, M. B., Berendse, F., and van der Zee, S. E. A. T. M.: Including hydrological self-regulating processes in peatland models: Effects on peatmoss drought projections, The Science of the total environment, 580, 1389–1400, doi:10.1016/j.scitotenv.2016.12.104, 2017.

Pastorello, G., Trotta, C., Canfora, E., Chu, H., Christianson, D., Cheah, Y.-W., Poindexter, C., Chen, J., Elbashandy, A., Humphrey, M., Isaac, P., Polidori, D., Reichstein, M., Ribeca, A., van Ingen, C., Vuichard, N., Zhang, L., Amiro, B., Ammann, C., Arain, M. A., Ardö, J., Arkebauer, T., Arndt, S. K., Arriga, N., Aubinet, M., Aurela, M., Baldocchi, D., Barr, A., Beamesderfer, E., Marchesini, L. B., Bergeron, O., Beringer, J., Bernhofer, C., Berveiller, D., Billesbach, D., Black, T. A., Blanken, P. D., Bohrer, G., Boike, J., Bolstad, P. V., Bonal, D., Bonnefond, J.-M., Bowling, D. R., Bracho, R., Brodeur, J., Brümmer, C., Buchmann, N., Burban, B., Burns, S. P., Buysse, P., Cale, P., Cavagna, M., Cellier, P., Chen, S., Chini, I., Christensen, T. R., Cleverly, J., Collalti, A., Consalvo, C., Cook, B. D., Cook, D., Coursolle, C., Cremonese, E., Curtis, P. S., D'Andrea, E., Da Rocha, H., Dai, X., Davis, K. J., Cinti, B. de, Grandcourt, A. de, Ligne, A. de, Oliveira, R. C. de, Delpierre, N., Desai, A. R., Di Bella, C. M., Di Tommasi, P., Dolman, H., Domingo, F., Dong, G., Dore, S., Duce, P., Dufrêne, E., Dunn, A., Dušek, J., Eamus, D., Eichelmann, U., ElKhidir, H. A. M., Eugster, W., Ewenz, C. M., Ewers, B., Famulari, D., Fares, S., Feigenwinter, I., Feitz, A., Fensholt, R., Filippa, G., Fischer, M., Frank, J., Galvagno, M., Gharun, M., Gianelle, D., Gielen, B., Gioli, B., Gitelson, A., Goded, I., Goeckede, M., Goldstein, A. H., Gough, C. M., Goulden, M. L., Graf, A., Griebel, A., Gruening, C., Grünwald, T., Hammerle, A., Han, S., Han, X., Hansen, B. U., Hanson, C., Hatakka, J., He, Y., Hehn, M., Heinesch, B., Hinko-Najera, N., Hörtnagl, L., Hutley, L., Ibrom, A., Ikawa, H., Jackowicz-Korczynski, M., Janouš, D., Jans, W., Jassal, R., Jiang, S., Kato, T., Khomik, M., Klatt, J., Knohl, A., Knox, S., Kobayashi, H., Koerber, G., Kolle, O., Kosugi, Y., Kotani, A., Kowalski, A., Kruijt, B., Kurbatova, J., Kutsch, W. L., Kwon, H., Launiainen, S., Laurila, T., Law, B., Leuning, R., Li, Y., Liddell, M., Limousin, J.-M., Lion, M., Liska, A. J., Lohila, A., López-Ballesteros, A., López-Blanco, E., Loubet, B., Loustau, D., Lucas-Moffat, A., Lüers, J., Ma, S., Macfarlane, C., Magliulo, V., Maier, R., Mammarella, I., Manca, G., Marcolla, B., Margolis, H. A., Marras, S., Massman, W., Mastepanov, M., Matamala, R., Matthes, J. H., Mazzenga, F., McCaughey, H., McHugh, I., McMillan, A. M. S., Merbold, L., Meyer, W., Meyers, T., Miller, S. D., Minerbi, S., Moderow, U., Monson, R. K., Montagnani, L., Moore, C. E., Moors, E., Moreaux, V., Moureaux, C., Munger, J. W., Nakai, T., Neirynck, J., Nesic, Z., Nicolini, G., Noormets, A., Northwood, M., Nosetto, M., Nouvellon, Y., Novick, K., Oechel, W., Olesen, J. E., Ourcival, J.-M., Papuga, S. A., Parmentier, F.-J., Paul-Limoges, E., Pavelka, M., Peichl, M., Pendall, E., Phillips, R. P., Pilegaard, K., Pirk, N., Posse, G., Powell, T., Prasse, H., Prober, S. M., Rambal, S., Rannik, Ü., Raz-Yaseef, N., Rebmann, C., Reed, D., Dios, V. R. de, Restrepo-Coupe, N., Reverter, B. R., Roland, M., Sabbatini, S., Sachs, T., Saleska, S. R., Sánchez-Cañete, E. P., Sanchez-Mejia, Z. M., Schmid, H. P., Schmidt, M., Schneider, K., Schrader, F., Schroder, I., Scott, R. L., Sedlák, P., Serrano-Ortíz, P., Shao, C., Shi, P., Shironya, I., Siebicke, L., Šigut, L., Silberstein, R., Sirca, C., Spano, D., Steinbrecher, R., Stevens, R. M., Sturtevant, C., Suyker, A., Tagesson, T., Takanashi, S., Tang, Y., Tapper, N., Thom, J., Tomassucci, M., Tuovinen, J.-P., Urbanski, S., Valentini, R., van der Molen, M., van Gorsel, E., van Huissteden, K., Varlagin, A., Verfaillie, J., Vesala, T., Vincke, C., Vitale, D., Vygodskaya, N., Walker, J. P., Walter-Shea, E., Wang, H., Weber, R., Westermann, S., Wille, C., Wofsy, S., Wohlfahrt, G.,

Wolf, S., Woodgate, W., Li, Y., Zampedri, R., Zhang, J., Zhou, G., Zona, D., Agarwal, D., Biraud, S., Torn, M., and Papale, D.: The FLUXNET2015 dataset and the ONEFlux processing pipeline for eddy covariance data, Scientific data, 7, 225, doi:10.1038/s41597-020-0534-3, 2020.

Pedregosa, F., Varoquaux, G., Gramfort, A., Michel, V., Thirion, B., Grisel, O., Blondel, M., Prettenhofer, P., Weiss, R., Dubourg, V., VanderPlas, J., Passos, A., Cournapeau, D., Brucher, M., Perrot, M., and Duchesnay, É.: Scikit-learn: Machine Learning in Python, Journal of Machine Learning Research, 2825–2830, 2011.

Rogiers, N., Eugster, W., Furger, M., and Siegwolf, R.: Effect of land management on ecosystem carbon fluxes at a subalpine grassland site in the Swiss Alps, Theor. Appl. Climatol., 80, 187–203, doi:10.1007/s00704-004-0099-7, 2005.

Runkle, B. R. K., Wille, C., Gažovič, M., Wilmking, M., and Kutzbach, L.: The surface energy balance and its drivers in a boreal peatland fen of northwestern Russia, Journal of Hydrology, 511, 359–373, doi:10.1016/j.jhydrol.2014.01.056, 2014.

Seabold, S. and Perktold, J.: Statsmodels: Econometric and Statistical Modeling with Python, 92–96, doi:10.25080/Majora-92bf1922-011.

Shekhar, A., Buchmann, N., Humphrey, V., and Gharun, M.: More than three-fold increase in compound soil and air dryness across Europe by the end of 21st century, Weather and Climate Extremes, 44, 100666, doi:10.1016/j.wace.2024.100666, 2024.

Song, L., Zhu, J., Li, X., Wang, K., Wang, G., and Sun, H.: Transpiration of Pinus sylvestris var. mongolica trees at different positions of sand dunes in a semiarid sandy region of Northeast China, Trees, 36, 749–762, doi:10.1007/s00468-021-02247-z, 2022.

Sonnentag, O., van der Kamp, G., Barr, A. G., and Chen, J. M.: On the relationship between water table depth and water vapor and carbon dioxide fluxes in a minerotrophic fen, Global change biology, 16, 1762–1776, doi:10.1111/j.1365-2486.2009.02032.x, 2010.

The pandas development team: pandas-dev/pandas: Pandas, doi:10.5281/zenodo.3509134, 2025.

Truong, C., Oudre, L., and Vayatis, N.: Selective review of offline change point detection methods, Signal Processing, 167, 107299, doi:10.1016/j.sigpro.2019.107299, 2020.

Türk, H., Stumpp, C., Stockinger, M., and Benettin, P.: Tracking Event-Scale Precipitation Partitioning Reveals Comparable Roles of Event Characteristics and Seasonality in Shaping Precipitation Fate in a Forested Landscape, Hydrological Processes, 40, doi:10.1002/hyp.70466, 2026.

Twine, T. E., Kustas, W. P., Norman, J. M., Cook, D. R., Houser, P. R., Meyers, T. P., Prueger, J. H., Starks, P. J., and Wesely, M. L.: Correcting eddy-covariance flux underestimates over a grassland, Agricultural and Forest Meteorology, 103, 279–300, doi:10.1016/S0168-1923(00)00123-4, 2000.

Utikal, J. and Rückriem, C.: Maßnahmenkonzept: Natura 2000 Amtsvenn und Hündfelder Moor DE-3807-301, in: Natura 2000-Gebiete in Nordrhein-Westfalen - Fachinformation - Listen der Natura 2000-Gebiete, Landesamt für Natur, Umwelt und Verbraucherschutz Nordrhein-Westfalen (Ed.), 2019.

van Rossum, G. and Drake, F. L.: Python 3 reference manual, CreateSpace, 2009.

Virtanen, P., Gommers, R., Oliphant, T. E., Haberland, M., Reddy, T., Cournapeau, D., Burovski, E., Peterson, P., Weckesser, W., Bright, J., van der Walt, S. J., Brett, M., Wilson, J., Millman, K. J., Mayorov, N., Nelson, A. R. J., Jones, E., Kern, R., Larson, E., Carey, C. J., Polat, İ., Feng, Y., Moore, E. W., VanderPlas, J., Laxalde, D., Perktold, J., Cimrman, R., Henriksen, I., Quintero, E. A.,

Harris, C. R., Archibald, A. M., Ribeiro, A. H., Pedregosa, F., and van Mulbregt, P.: SciPy 1.0: fundamental algorithms for scientific computing in Python, Nature methods, 17, 261–272, doi:10.1038/s41592-019-0686-2, 2020.

Wilusz, D. C., Harman, C. J., and Ball, W. P.: Sensitivity of Catchment Transit Times to Rainfall Variability Under Present and Future Climates, Water Resources Research, 53, 10231–10256, doi:10.1002/2017WR020894, 2017.

Wutzler, T., Lucas-Moffat, A., Migliavacca, M., Knauer, J., Sickel, K., Šigut, L., Menzer, O., and Reichstein, M.: Basic and extensible post-processing of eddy covariance flux data with REddyProc, Biogeosciences, 15, 5015–5030, doi:10.5194/bg-15-5015-2018, 2018.

Xu, J., Wu, B., Ryu, D., Yan, N., Zhu, W., and Ma, Z.: Quantifying the contribution of biophysical and environmental factors in uncertainty of modeling canopy conductance, Journal of Hydrology, 592, 125612, doi:10.1016/j.jhydrol.2020.125612, 2021.

Yu, Z. C.: Northern peatland carbon stocks and dynamics: a review, Biogeosciences, 9, 4071–4085, doi:10.5194/bg-9-4071-2012, 2012.

Yuan, W., Zheng, Y., Piao, S., Ciais, P., Lombardozzi, D., Wang, Y., Ryu, Y., Chen, G., Dong, W., Hu, Z., Jain, A. K., Jiang, C., Kato, E., Li, S., Lienert, S., Liu, S., Nabel, J. E. M. S., Qin, Z., Quine, T., Sitch, S., Smith, W. K., Wang, F., Wu, C., Xiao, Z., and Yang, S.: Increased atmospheric vapor pressure deficit reduces global vegetation growth, Science advances, 5, eaax1396, doi:10.1126/sciadv.aax1396, 2019.

Zhang, Y., Liu, X., Wang, K., Zhang, D., and Liu, W.: Widespread Increasing Control of Water Supply on Evapotranspiration, Water Resources Research, 60, doi:10.1029/2024WR038353, 2024.